New design techniques on matching couplers for traveling-wave accelerating structures

Zhicheng Huang, Yelong Wei,* Zexin Cao, Li Sun, and Guangyao Feng
National Synchrotron Radiation Laboratory, University of Science and Technology of China, Hefei, China

David Alesini
INFN Frascati National Laboratories, Frascati, Rome, Italy

(Received 24 January 2024; accepted 17 July 2024; published 5 August 2024)

Numerical optimizations on couplers of the traveling-wave (TW) accelerating structures usually require lots of calculation resources. This paper proposes a new technique for matching couplers to an accelerating structure in a more efficient and accurate way. It combines improved Kroll method with improved Kyhl method, thereby simplifying simulation process while achieving a high accuracy. This paper also presents the detailed design on couplers for a C-band constant-gradient (CG) accelerating structure based on this new technique. Such a new technique can be widely used for any TW accelerating structures working at different frequencies of S-band, C-band, and X-band including CG, constant-impedance (CI), and other structures with either electric couplers or magnetic couplers.

DOI: 10.1103/PhysRevAccelBeams.27.082001

I. INTRODUCTION

There has been a major effort to develop radiofrequency (rf) technology that is capable of producing high accelerating gradients over the past few decades. This technology includes S-band, C-band, and X-band traveling-wave (TW) accelerating structures. S-band and C-band accelerating structures usually generate gradients of 20–30 MV/m [1–4] and 30–50 MV/m [5–9], respectively, while X-band structures have obtained a gradient of 120 MV/m with a pulse length of 200 ns [10–13]. For the realization of these TW structures, it is of particular importance to carefully design the couplers so that rf power is smoothly transmitted into and out of the structure with negligible reflections. It usually requires lots of simulation time for design of input and output couplers.

A TW structure consists of a finite number of regular accelerating cells and two couplers. Couplers can be defined as "electric" or "magnetic" coupling, depending on which type of field is coupled [14–15]. Each coupler has a matching cell which is used for the matching between regular cells and couplers. Different matching techniques have been proposed and studied on the couplers over the past few decades. One of the most representative techniques is the equivalent circuit analysis. In 1963, Kyhl and Westbrook proposed an equivalent circuit model to measure the matching of couplers for a TW structure working at $2\pi/3$ mode [16]. In this method, a metallic tuner is moved to the center of the accelerating cells so that they are short-circuited. Then the phases of global reflection coefficient at frequencies for the $\pi/2$ mode and the $2\pi/3$ mode are utilized to guide the adjusting direction of matching of couplers to a TW structure. Since then, this method is called the Kyhl method. In 1993, Kyhl method has been further studied and extended to the matching of the couplers to TW structures at any operating mode by Chanudet [17]. It allows the input and output couplers to be designed separately while the accelerating cells do not have to be exactly tuned. In 2007, Alesini *et al.* [18] simplified the equivalent circuit model to minimize the amplitudes of global reflection coefficient from the input waveguide for the matching of couplers to a TW structure. Zheng *et al.* [19] derived the detailed quantitative equations for Kyhl method instead of only giving the adjusting direction in the process of matching couplers by using the coupling coefficient $\beta \to 1$ and frequency deviation $\Delta f \to 0$ as the design target for the matching couplers to a TW structure. Afterward, this method has been widely used in present coupler designs for TW structures. For example, Zhang *et al.* at IHEP designed a $3\pi/4$-mode C-band structure based on Kyhl method [20]. Kyhl method works to some extent for a constant-impedance (CI) structure as the regular cell keeps constant for the whole structure. However, an arbitrary reference of the coupler's shorting position and approximation errors lead to some uncertainty.

*Contact author: wylong@ustc.edu.cn

The variations of regular cells might also result in a poor optimization accuracy especially for a non-CI structure (see Appendix B). In this case, the matching dimensions are not that accurate using Kyhl method. So other methods have to be considered to improve the accuracy on the matching of couplers.

In 1990s, another approach was proposed for coupler design by researchers at SLAC. Ng *et al.* described a numerical simulation procedure for coupler design with focusing on the scattering parameters of the whole TW structure [21–22]. But the procedure for the tapered or asymmetric structures was very complicated on account of its multiobjective optimization process. Then Kroll *et al.* proposed a new method that utilizes local reflection coefficient for matching instead of simulating the global reflection coefficient [23]. It should also be noted that this method is called the Kroll method in the following. In this situation, the input and output couplers can be independently designed for the matching process. This greatly simplifies the whole optimization procedure while achieving the accuracy. Kroll method has also been widely used in the design of TW structures worldwide. For example, Fang *et al.* at SINAP employed it to design the couplers of their C-band structures [24]. Grudiev *et al.* at CERN utilized this method to design their X-band TW structures for CLIC [25–28]. Although Kroll method has greatly simplified matching process, we still spend lots of time on sweeping multiple geometrical parameters for finding optimum dimensions.

In order to resolve these issues, we propose a new technique combining Kyhl method and Kroll method for efficient coupler design in this paper. This new technique greatly reduces the optimization time as well as achieving a high accuracy. The couplers for a C-band TW structure are designed by such a new technique. In Sec. II, both improved Kroll and Kyhl methods for designing couplers are analyzed in detail. In Sec. III, a new technique is proposed and studied with an example of C-band structure. Section IV gives summary and outlook.

II. COUPLER MATCHING TECHNIQUES BY IMPROVED KROLL AND KYHL METHODS

A TW structure working at a mode of φ, consists of an input coupler, four regular cells and an output coupler, as shown in Fig. 1. Each coupler includes a waveguide and a matching cell. The matching cells have different coupling apertures and cell diameters. The rf power is transmitted into and out of the structure through input and output couplers, respectively. The matching cells are utilized to achieve matching between the regular cells and couplers so that rf power is transmitted into and out of regular cells with negligible reflections. The optimizations focus on the coupling apertures a_{ci}, a_{co} and matching cell diameters b_{ci}, b_{co}, aiming to minimize the global reflection coefficient $|S_{11}|$ at the input port and to maximize global transmission coefficient $|S_{21}|$ from the input port to the output port. It should be noted that the global reflection coefficient $|S_{11}|$ is defined as looking into the input coupler from its waveguide port in this paper.

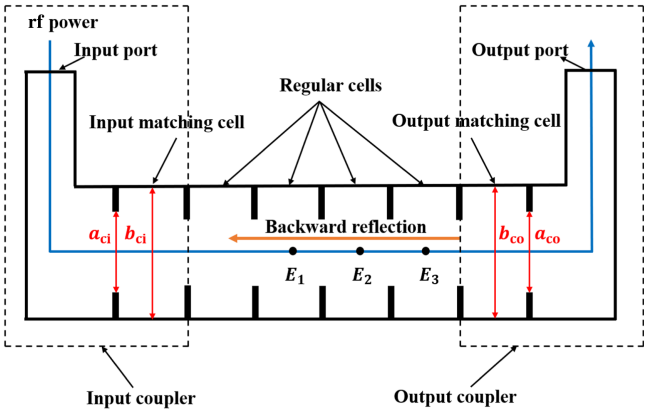

FIG. 1. The sketch of a TW structure consisting of an input coupler, four regular cells, and an output coupler.

A. Improved Kroll method

In this section, Kroll method is described in detail for the optimizations on the matching cells with coupling apertures and matching cell diameters. It allows the input and output matching cells to be designed independently. The local reflection can be calculated from the simulated electric fields on the beam axis. The longitudinal electric fields at the center of three consecutive cells adjacent to the matching cell, denoted as E_1, E_2, and E_3 in Fig. 1, are represented by the following equations:

$$E_1 = E_0(e^{j\varphi} + |R|e^{j(\theta-\varphi)}), \tag{1}$$

$$E_2 = E_0(1 + |R|e^{j\theta}), \tag{2}$$

$$E_3 = E_0(e^{-j\varphi} + |R|e^{j(\theta+\varphi)}), \tag{3}$$

where $E_0 = |E_0|e^{j\alpha_0}$, $R = |R|e^{j\theta}$, $|E_0|$ is the amplitude of forward fields, α_0 is the initial phase of forward fields, $|R|$ is the amplitude of local reflection (20 log $|R|$ is called as the local reflection coefficient in the whole paper), θ is the phase of local reflection, and φ is the phase advance between regular cells. $|E_0|$ and $|R|$ are the constants when the structure is assumed to be lossless. Based on the above equations and assumptions, the following definitions are used to obtain R and φ for coupler design:

$$\Delta = \frac{E_3 - E_1}{2E_2}, \tag{4}$$

$$\Sigma = \frac{E_3 + E_1}{2E_2}, \tag{5}$$

$$\varphi = \cos^{-1}\Sigma, \tag{6}$$

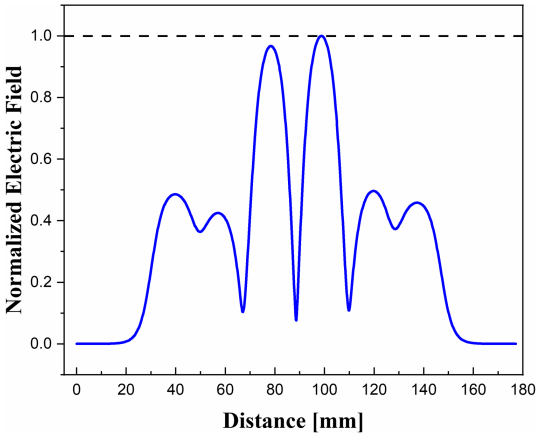

FIG. 2. The worse electric field flatness caused by a local reflection coefficient $20\log|R| = -4$ dB.

$$R = \frac{\sin\varphi - j\Delta}{\sin\varphi + j\Delta}. \tag{7}$$

In contrast to previous methods using the scattering parameters (S_{11} and S_{21}) for the whole structure, Kroll method focuses on the optimizations of the output coupling aperture a_{co} and cell diameter b_{co} to achieve $|R| \to 0$. When $|R|$ approaches zero, Δ converges to $-j\sin\varphi$ and Σ converges to $\cos\varphi$ through Eqs. (4)–(7). One purpose of achieving $|R| \to 0$ is to obtain good field flatness and little disturbance on the cell-to-cell phase advance. When the output matching cell is not well designed, the local reflection results in a worse field flatness, as illustrated in Fig. 2. The other purpose of achieving $|R| \to 0$ is to avoid spurious matching that can be easily caused by the cancellation of reflected waves from the input coupler and output coupler. In the case of spurious matching, backward waves still persist in the structure although there is no reflection at the input port. Therefore, it is necessary to achieve $|R| \to 0$ in order to eliminate any reflections from the output coupler. Afterward, the optimizations on the input coupling aperture a_{ci} and matching cell diameter b_{ci} are performed to achieve the global reflection coefficient $|S_{11}| \to 0$ at the input port.

The above optimization process is based on the assumptions that $|E_0|$ and $|R|$ are constant. However, these assumptions are often not satisfied for most of TW structures, such as a CI structure. This might dilute the accuracy of Kroll method. It is found that the optimization accuracy is mainly affected by the case of when $|E_0|$ is not constant while the case of when $|R|$ is not constant does not have any impact on its accuracy. This has been discussed in detail in Appendix A.

In order to improve Kroll method for any TW structures including constant-gradient (CG) and non-CG structures, we propose a new criterion R' that focuses on the phases θ_1, θ_2, and θ_3 of the axial longitudinal electric fields E_1, E_2, and E_3 at the center of three consecutive cells, as shown in Fig. 1. For a TW structure, in which $|E_0|$ is not constant in Eqs. (1)–(3), E_1, E_2, and E_3 are rewritten as

$$E_1 = |E_1|e^{j\theta_1} = E_{01}(e^{j\varphi} + |R'|e^{j(\theta-\varphi)}), \tag{8}$$

$$E_2 = |E_2|e^{j\theta_2} = E_{02}(1 + |R'|e^{j\theta}), \tag{9}$$

$$E_3 = |E_3|e^{j\theta_3} = E_{03}(e^{-j\varphi} + |R'|e^{j(\theta+\varphi)}), \tag{10}$$

where $E_{01} = |E_{01}|e^{j\alpha_0}$, $E_{02} = |E_{02}|e^{j\alpha_0}$, $E_{03} = |E_{03}|e^{j\alpha_0}$, $|E_{01}|$, $|E_{02}|$, and $|E_{03}|$ are the amplitudes of forward fields, α_0 is the initial phase of forward fields, R' is defined as the local reflection, $R' = |R'|e^{j\theta}$, $|R'|$ is the amplitude of local reflection, θ is the phase of local reflection, and φ is the phase advance between regular cells. It should be noted here that $|R'|$ is assumed to be constant, which does not have any effect on the accuracy of Kroll method.

The phases of E_1, E_2, and E_3 can be expressed as

$$\arg E_1 = \arg(E_{01}e^{j\varphi}) + \arg(1 + |R'|e^{j(\theta-2\varphi)}), \tag{11}$$

$$\arg E_2 = \arg E_{02} + \arg(1 + |R'|e^{j\theta}), \tag{12}$$

$$\arg E_3 = \arg(E_{03}e^{-j\varphi}) + \arg(1 + |R'|e^{j(\theta+2\varphi)}). \tag{13}$$

Here the symbol "arg" is used to denote the phase of a complex number. An approximation equation based on the first-order Taylor expansion is utilized as follows:

$$\arg(1 + Ae^{j\alpha}) \approx A\sin\alpha, \tag{14}$$

where A is a real value much smaller than 1, and α is an arbitrary angle. By using Eq. (14), we obtain the phases as follows:

$$\theta_1 \approx \alpha_0 + \varphi + |R'|\sin(\theta - 2\varphi), \tag{15}$$

$$\theta_2 \approx \alpha_0 + |R'|\sin\theta, \tag{16}$$

$$\theta_3 \approx \alpha_0 - \varphi + |R'|\sin(\theta + 2\varphi), \tag{17}$$

where φ is the phase advance between regular cells, and it can be calculated by the real part of Σ. Combining Eqs. (15)–(17), we obtain:

$$\theta_3 - \theta_2 = -\varphi + |R'|(\sin(\theta + 2\varphi) - \sin\theta), \tag{18}$$

$$\theta_2 - \theta_1 = -\varphi + |R'|[\sin\theta - \sin(\theta - 2\varphi)]. \tag{19}$$

Then the phase θ and amplitude $|R'|$ of the local reflection can be obtained:

$$\theta = \arctan\left(\frac{2\theta_2 - \theta_1 - \theta_3}{\theta_3 + 2\varphi - \theta_1}\cot\varphi\right), \tag{20}$$

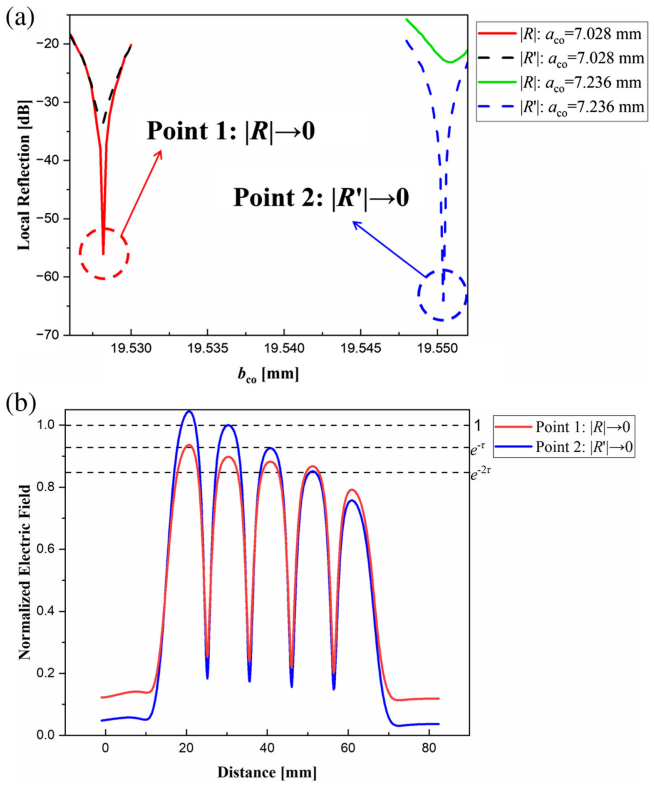

FIG. 3. (a) The relationship of local reflection coefficients $20\log|R|$ and $20\log|R'|$ with a_{co} and b_{co} for a CI structure. (b) The normalized longitudinal electric fields for optimum structures corresponding to point 1 and point 2 [see (a)], respectively. τ is the attenuation factor for the regular cell.

$$|R'| = \left|\frac{\theta_3 - \theta_1 + 2\varphi}{2\cos\theta \sin 2\varphi}\right|. \tag{21}$$

Therefore, the optimization target is to achieve $|R'| \to 0$, which is a new criterion as a substitution of $|R| \to 0$.

A new criterion $|R'| \to 0$ [Eq. (21)] and an original criterion $|R| \to 0$ [Eq. (7)] are utilized for the optimizations on a CI structure, which is an example of non-CG structures. It can be found that $|R'|$ and $|R|$ are different to each other for the same dimensions. As shown in Fig. 3(a), when $|R'| \to 0$, the optimum values of a_{co} and b_{co} corresponding to point 2 are quite different with those of $|R| \to 0$ corresponding to point 1. The simulated electric fields from point 1 and point 2, respectively, are compared with the theoretical calculated fields for a CI structure, as shown in Fig. 3(b). It can be clearly seen that the electric fields from point 2 corresponding to $|R'| \to 0$ has an agreement with the theoretical fields much better than those from point 1 corresponding to $|R| \to 0$. This means that the new criterion $|R'| \to 0$ achieves an accuracy much better than that of the original criterion $|R| \to 0$ for CI structures. It can be expected that this new criterion $|R'| \to 0$ also works for other TW structures, in which the accelerating fields are not constant and gradually rise, such as an unloaded CLIC

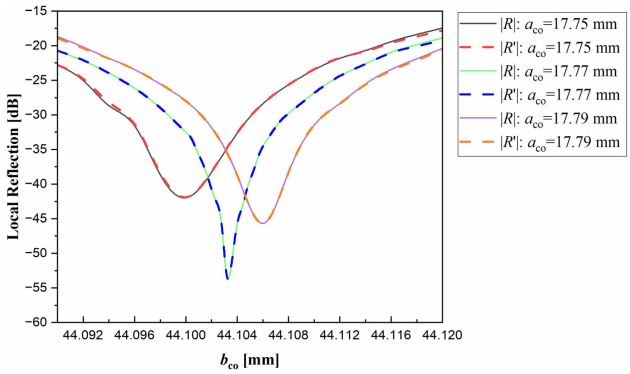

FIG. 4. The relationship of local reflection coefficients $20\log|R|$ and $20\log|R'|$ with a_{co} and b_{co} for a CG structure.

structure [25–28]. Both criterions are also applied for optimizations on a CG structure. It is found that both criterions generate the same dimensions for matching couplers, as shown in Fig. 4. This means that both criterions work for optimizations on CG structures at a same accuracy. Based on these studies, the new criterion $|R'| \to 0$ improves and enables Kroll method for optimizations on couplers to any TW structures including CG, CI, and other structures.

The optimizations on a_{co} and b_{co} usually take a large amount of time in order to achieve a local reflection coefficient $20\log|R'| \leq -45$ dB, which usually meets the requirement of realistic tuning. Parameter sweeping has to be performed using different a_{co} and b_{co}, as shown in Fig. 4. It can be also found in Fig. 4 that the optimum a_{co} and b_{co} exhibit a narrow passband, which is typically in the order of 50 μm. Such a narrow passband may result in a time-consuming iterative process starting from random dimensions of a_{co} and b_{co}. It is of particular importance to find a good starting point for a_{co} and b_{co} using this improved Kroll method.

B. Improved Kyhl method

In contrast to Kroll method, the phases of the global reflection coefficient at different frequencies are utilized to achieve matching by Kyhl method. Kyhl method allows to match the couplers separately from the cell chain in the design process. For a CI structure, Kyhl method works to some extent as the regular cell keeps constant for the whole cell chain. For a non-CI structure, the variations of regular cells might result in a poor optimization accuracy for Kyhl method. This has been described in detail in Appendix B.

Here we take the output coupler as an example to describe Kyhl method. It also works for the design of input coupler. The regular cell adjacent to the output matching cell is simulated to obtain the frequencies for $\pi/2$ mode and φ mode, denoted as f_1 and f_2, respectively. First, a metallic plunger is moved to the center of the matching cell so that it is short-circuited. The phases of

global reflection coefficient at f_1 and f_2 are denoted as φ_{m1} and φ_{m2}, respectively. It should be noted that f_1 and f_2 can be any frequencies within the passband. Subsequently, the metallic plunger is moved to the center of the adjacent regular cell. The phases of global reflection coefficient at f_1 and f_2 are denoted as φ_{n1} and φ_{n2}, respectively. The phase advances between the regular cell and the matching cell are denoted as φ_1 and φ_2:

$$\varphi_1 = \varphi_{n1} - \varphi_{m1}, \tag{22}$$

$$\varphi_2 = \varphi_{n2} - \varphi_{m2}. \tag{23}$$

Then φ_1 and φ_2 are used to calculate the coupling coefficient β and the frequency deviation Δf of the matching cell by the following equations:

$$\beta = \frac{\tan\frac{\varphi_1}{2}\tan\frac{\varphi_2}{2}(f_1 + f_2)}{\tan\varphi(\tan\frac{\varphi_1}{2}f_2 - \tan\frac{\varphi_2}{2}f_1)}, \tag{24}$$

$$f_{\mathrm{co}} = \frac{f_1 + f_2}{2}, \tag{25}$$

$$\Delta f = \sqrt{f_1 f_2}\sqrt{\frac{\tan\frac{\varphi_2}{2}f_2 - \tan\frac{\varphi_1}{2}f_1}{\tan\frac{\varphi_2}{2}f_1 - \tan\frac{\varphi_1}{2}f_2}} - f_{\mathrm{co}}. \tag{26}$$

These equations are derived with some mathematical approximations. However, it allows the output coupler to be optimized for matching by targeting $\beta \to 1$ and $\Delta f \to 0$.

Throughout the optimization process, it is observed that β is significantly affected by a_{co}, while Δf is simultaneously influenced by both b_{co} and a_{co}. In this situation, a common strategy is to adjust a_{co} to achieve $\beta \to 1$, and then b_{co} is fine-tuned for $\Delta f \to 0$. Compared to the iterations required by Kroll method, Kyhl method runs much faster with a common starting point. However, it is still very time-consuming and takes dozens of iterations to achieve convergence by Kyhl method. Therefore, we propose a new strategy to greatly reduce the number of iterations so that it saves lots of simulation time.

This new strategy is based on a linear analysis model [29–30]. This model requires a linearity between β, Δf and a_{c}, b_{c} for fast convergence. Based on the model, it can be expressed as follows:

$$P = [\mathrm{d}\beta \quad \mathrm{d}(\Delta f)]^T, \tag{27}$$

$$Q = [\Delta a_{\mathrm{c}} \quad \Delta b_{\mathrm{c}}]^T, \tag{28}$$

$$W = \begin{bmatrix} \frac{\partial\beta}{\partial a_{\mathrm{c}}} & \frac{\partial\beta}{\partial b_{\mathrm{c}}} \\ \frac{\partial(\Delta f)}{\partial a_{\mathrm{c}}} & \frac{\partial(\Delta f)}{\partial b_{\mathrm{c}}} \end{bmatrix}, \tag{29}$$

$$P = WQ, \tag{30}$$

where P represents the variations of β and Δf. The Jacobi matrix W can be obtained using finite difference between these two sets of variables.

In a linear model, traditional gradient descent algorithms have some limitations in terms of low efficiency and divergence [31–32]. With the aim of achieving convergence in as few iterations as possible, a line search algorithm is utilized to optimize the linear model [33–34]. In this case, the initial values can be arbitrarily chosen. The updated equation is as follows:

$$x_k = [a_{ck} \quad b_{ck}]^T, \tag{31}$$

$$y_k = [\beta_k \quad \Delta f_k]^T, \tag{32}$$

$$y_0 = [1 \quad 0]^T, \tag{33}$$

$$x_{k+1} - x_k = \eta W^{-1}(y_0 - y_k), \tag{34}$$

where a_{ck}, b_{ck}, β_k, Δf_k represent the coupling aperture, matching cell diameter, coupling coefficient, and frequency

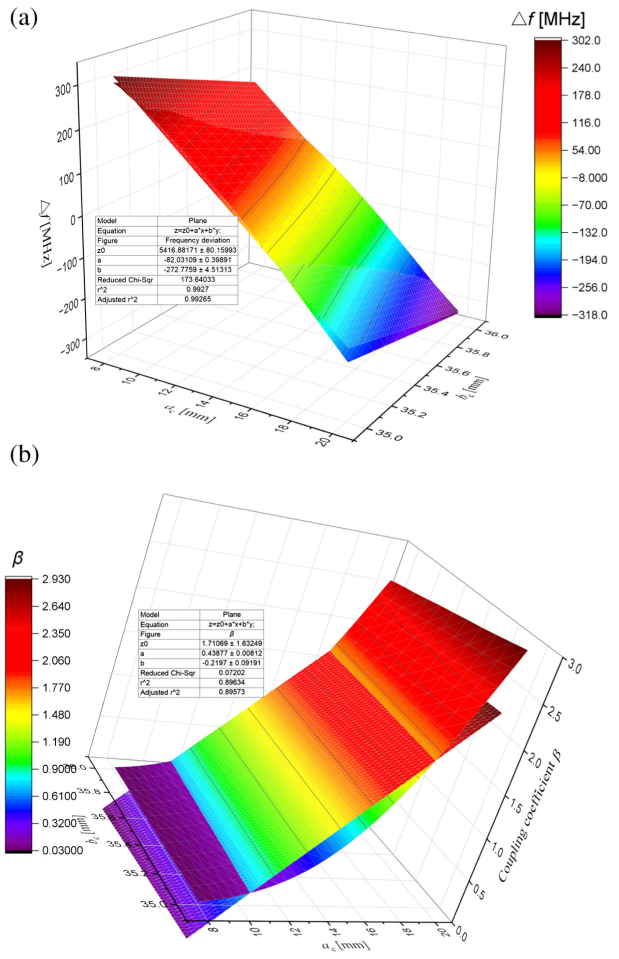

FIG. 5. (a) Δf and (b) β as a function of a_{c} and b_{c}. Each 3D-plot is inserted with a linear fitting plane and r^2 denotes the fitting accuracy between a simulated plane and a fitting plane. When r^2 is close to 1, the simulated plane has a good linearity on a_{c} and b_{c}.

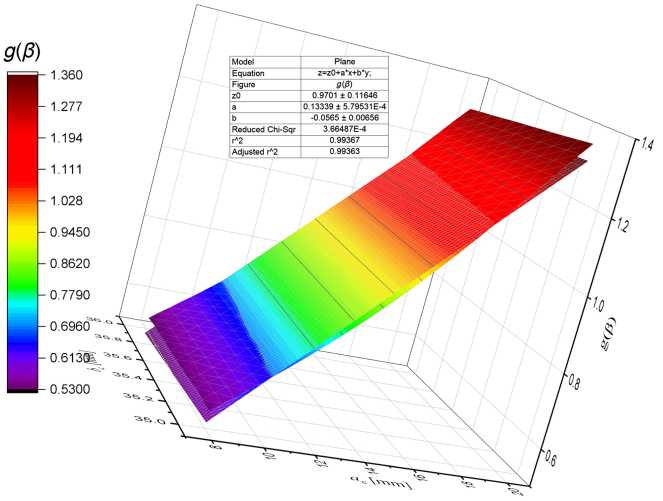

FIG. 6. $g(\beta)$ as a function of a_c and b_c, it is inserted with a linear fitting plane and r^2 denotes the fitting accuracy between a simulated plane and a fitting plane.

deviation in the kth iteration. The descent direction is chosen as ηW^{-1}, the step length is chosen as $y_0 - y_k$, and the learning rate η is set to 1. By this equation, the linear model achieves convergence in just a few iterations with a good linearity of W. It should be noted that W can be only initialized once in the simulations.

Figure 5 shows three-dimensional (3D) plots for the dependences of Δf and β on a_c and b_c. It can be clearly seen in Fig. 5(a) that Δf has a good linearity on a_c and b_c. It can be also found that β has a linearity on b_c while β does not have a linearity on a_c within a broad range through simulations, as shown in Fig. 5(b). This may result in divergence in a linear model with a line search algorithm.

In order to improve the efficiency for our optimization process, an algebraic transformation [35] is required to improve the linearity between β and a_c. This transformation aims to mitigate the impact of nonlinearities and increase the overall linearity of the model. Based on the simulations in Fig. 5, an algebraic transformation is applied to β:

$$g(\beta) = \frac{\ln(1+h)}{\ln(1+\frac{h}{\beta})}. \tag{35}$$

The function g is continuously differentiable within the range of β. In our case, h is chosen to be 50, which is enough to generate a good linearity. It can be seen in Fig. 6

TABLE I. Fitting accuracy of Δf, β, and $g(\beta)$ for different couplers.

	Fitting accuracy r^2		
TW structures	Δf	β	$g(\beta)$
Electric coupler	0.972	0.840	0.974
Magnetic coupler	0.993	0.896	0.994

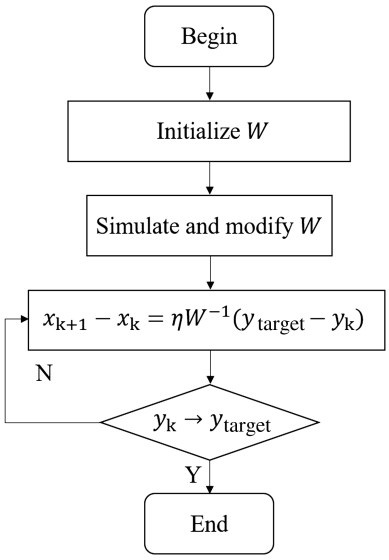

FIG. 7. The optimization program flowchart with the line search algorithm.

that $g(\beta)$ has a good linearity on a_c and b_c. It ultimately expedites the overall optimization process by Kyhl method. Table I shows the fitting accuracy of Δf, β, and $g(\beta)$ for TW structures with electric and magnetic couplers. It can be found that $g(\beta)$ has a linearity much better than that of β on a_c and b_c for both couplers. This verifies the validity of the transformation.

The optimization flowchart is shown in Fig. 7. We have written a python script to drive HFSS solver [36] for the optimizations on the dimensions of couplers in an automated fashion. As for the typical geometries, the script can converge in just a few iterations, regardless of the parameter initialization.

III. NEW MATCHING TECHNIQUE

In this section, a new technique combining improved Kyhl method and Kroll method is proposed and studied on couplers for TW accelerating structures. Based on the analysis and improvements on these two methods, in order to verify such a new technique, a C-band CG accelerating

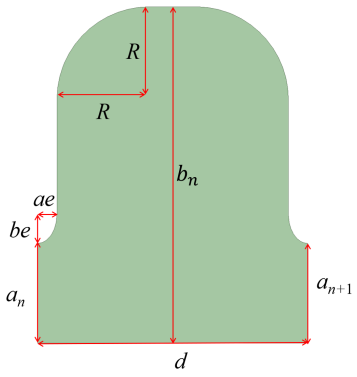

FIG. 8. The cell geometry with elliptical fillets and curved tops.

TABLE II. Parameters of the whole C-band structure.

Parameters	Value	Unit
Operating frequency f	5712	MHz
Operating mode	$3\pi/4$	rad
Number of cells	$44+2$	
Cell length d	19.682	mm
Disk thickness $2ae$	2.5	mm
Iris $2a$	$12.5-10.466$	mm
Cell diameter $2b$	$43.837-43.374$	mm
Shunt impedance R_s	$89.6-98.5$	MΩ/m
Quality factor Q	$12022-11959$	
Group velocity v_g/c	$1.585\%-0.848\%$	c
Filling time t_f	253	ns
Attenuation factor τ	0.3781	

structure working at $3\pi/4$ mode is utilized as an example. The cell geometry consists of elliptical fillets and curved tops, as illustrated in Fig. 8. Through optimizations, the rf parameters for the whole structure are listed in Table II. The electric couplers are adopted to transmit rf power into and out of the structure.

The new technique combines improved Kyhl method and improved Kroll method for the optimizations on the couplers (focus on the matching cells). In order to avoid spurious matching, the output coupler is optimized first using this new technique. A short C-band structure consisting of an input coupler, four regular cells, and an output coupler is modeled for the simulations, as shown in Fig. 9. It should be noted here that the regular cells are the four last cells adjacent to the output matching cell while the input coupler is only for this short structure rather than for the whole structure. In the first step, improved Kyhl method is utilized to optimize the coupling aperture a_{co} and cell diameter b_{co}. By moving a metallic plunger into the center of sixth and fifth cells, respectively, the coupling coefficient β_{out} and frequency deviation Δf_{out} can be obtained using Eqs. (8)–(12). A linear model as described

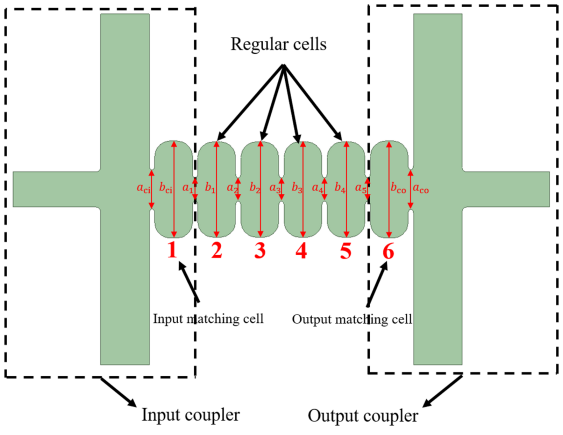

FIG. 9. The modeling of a short C-band structure consisting of an input coupler, four regular cells, and an output coupler.

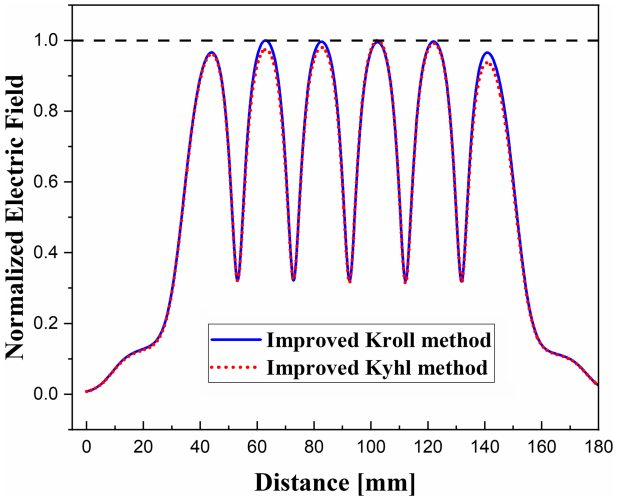

FIG. 10. The normalized electric fields simulated by improved Kroll and Kyhl methods. The red curve denotes fields by improved Kyhl method while the blue curve denotes fields by improved Kroll method.

in Sec. II is employed for the optimizations on the coupling aperture a_{co} and cell diameter b_{co}. It only takes a few iterations to converge even for arbitrary initial values of $\beta_{\mathrm{out}}=0.777$ and $\Delta f_{\mathrm{out}}=151.04$ MHz, as shown in Table II. After achieving convergence by improved Kyhl method, the longitudinal electric fields on the beam axis are depicted as red curve in Fig. 10. Using Eqs. (15)–(21), these electric fields exhibit a local reflection coefficient $20\log|R'|=-36$ dB. Such a reflection may cause a phase disturbance for each cell, thus affecting the matching of input coupler. To address this issue, further optimization is required by improved Kroll method. Given that improved Kyhl method has already brought the variations of a_{co} and b_{co} into the passband, very close to the desired matching dimensions, only a few iterations are required to converge for the final matching. So in the next step, the improved Kroll method is employed to achieve a perfect matching using the starting points from improved Kyhl method. After optimizations by improved Kroll method, the longitudinal electric field on the beam axis is depicted as blue curve in Fig. 10. In this case, we obtain a local reflection coefficient $20\log|R'|=-56$ dB, which improves a lot as compared with that of improved Kyhl method. Due to the asymmetry of the structure (variations of regular cells) and approximation in Kyhl method, the output coupler is actually undercoupled, as indicated in Table III. These simulations take about 2–3 h to get very accurate dimensions for the output coupler using the new technique even on a common private computer. This is much faster than that of only using Kroll method which may take about several days to sweep parameters for this structure.

After optimizations on the output coupler for the whole structure, we use the same technique to design the input coupler (focus on the input matching cell). Another short

TABLE III. Optimization process of the output coupler.

Iteration	a_{co} (mm)	b_{co} (mm)	β	Δf (MHz)	$\lvert R'\rvert$ (dB)		Methods
1	16.600	43.0000	0.777	151.04	⋯	Initialization	Improved Kyhl method
2	16.766	43.0000	0.835	155.07	⋯	Initialize the first column of W	
3	16.766	44.0544	0.647	−13.09	⋯	Initialize the second column of W	
4	17.810	44.1314	0.974	−3.31	⋯	Optimization	
5	17.870	44.1198	1.000	−0.22	⋯	Optimization	
6	17.870	44.1184	1.000	0.01	−36	Converge	
7	17.770	44.1032	0.964	0.16	−56	Refinement	Improved Kroll method

C-band structure consisting of an input coupler, four regular cells, and an output coupler is modeled for the simulations. In this case, the regular cells are the four first cells adjacent to the input matching cell while the output coupler is only for this short structure rather than for the whole structure. Through sweeping different coupling aperture a_{ci} and matching cell diameter b_{ci}, the global reflection coefficient $|S_{11}|$ can be minimized at the input port. Thus the optimum dimensions can be obtained for the input matching cell. It should be noted that the couplers can be either electric or magnetic couplers. In conclusion, this new technique greatly simplifies the design process and achieves a high accuracy for matching couplers to this C-band structure.

IV. SUMMARY

In this paper, a new criterion $|R'| \to 0$ is proposed to improve and enable Kroll method to work for any TW structures, including CG, CI, and other structures. We have also improved Kyhl method using a linear model, which greatly reduces calculation time. This improved Kyhl method can be used to combine with improved Kroll method to form a new design technique on couplers for TW accelerating structures. Such a new technique greatly simplifies optimization process and achieves high accuracy. The couplers of a C-band accelerating structure have been designed by this new technique. It takes only several hours to complete the whole structure design. As compared with the existing matching methods which usually take about several weeks, our new technique is more efficient.

This new technique can be widely used for any TW accelerating structures working at different frequencies of S-band, C-band, and X-band including CG, CI, and other structures with either electric couplers or magnetic couplers. It is also foreseen that a new tuning strategy can be also formed based on this new technique. This will be reported in separate publications.

ACKNOWLEDGMENT

The authors would like to thank Dr. Alexej Grudiev and Dr. Ping Wang at CERN for fruitful discussions. This work is supported by the "Hundred Talents Program" of the Chinese Academy of Sciences (Grant No. KJ2310007003), the Fundamental Research Funds for the Central Universities (Grants No. WK2310000114, No. KY2310000047, and No. KY2310000067), Hefei Advanced Light Facility project, and STCF Key Technology Research project.

APPENDIX A

For TW accelerating structures, the accelerating gradient E for a regular cell can be expressed as follows:

$$P_{out} = P_{in} e^{-\frac{\omega d}{Q v_g}}, \tag{A1}$$

$$E^2 = \frac{\omega R_s P_{in}}{Q v_g}, \tag{A2}$$

where P_{in}, P_{out}, ω, d, Q, v_g, and R_s represent the input power, output power, angular frequency, cell length, unloaded quality factor, group velocity, and shunt impedance for a regular cell, respectively. Figure 11 shows the rf wave propagating through three consecutive regular cells.

(i) When these these consecutive regular cells form a CG structure, we can obtain the following equations using Eqs. (A1)–(A2):

$$\frac{\omega P R_s}{Q v_{g1}} = \frac{\omega P R_s e^{-\frac{\omega d}{Q v_{g1}}}}{Q v_{g2}}, \tag{A3}$$

$$\frac{\omega P R_s}{Q v_{g2}} = \frac{\omega P R_s e^{-\frac{\omega d}{Q v_{g2}}}}{Q v_{g3}}, \tag{A4}$$

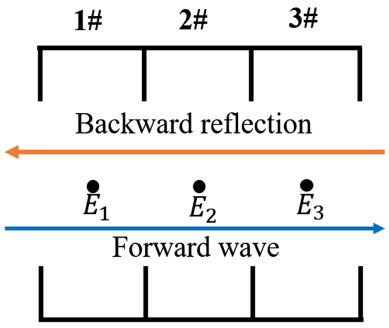

FIG. 11. The sketch of an rf wave propagating through three consecutive regular cells.

where P is the input power for the first cell, which is denoted as 1, v_{gi} is the group velocity for the ith cell ($i = 1, 2, 3$), Q and R_s are assumed to be constant for each cell. For a CG structure, Eqs. (1)–(3) from an original Kroll method can be modified as

$$E_1 = E_0(e^{j\varphi} + |R_1|e^{j(\theta-\varphi)}), \tag{A5}$$

$$E_2 = E_0(1 + |R_2|e^{j\theta}), \tag{A6}$$

$$E_3 = E_0(e^{-j\varphi} + |R_3|e^{j(\theta+\varphi)}), \tag{A7}$$

where $|R_i|$ is the amplitude of local reflections for the ith cell ($i = 1, 2, 3$). The local reflections for the ith cell are calculated by Eq. (A2):

$$|R_i^2|E_0^2 = \frac{\omega P_{\text{refi}} R_s}{Q v_{gi}}, \tag{A8}$$

$$P_{\text{ref}\,1} = P_{\text{ref}\,2} e^{-\frac{\omega d}{Q v_{g2}}} = P_{\text{ref}\,3} e^{-\frac{\omega d}{Q v_{g2}} - \frac{\omega d}{Q v_{g3}}}. \tag{A9}$$

Using Eqs. (A3), (A4) and (A8), (A9), we obtain the following equations:

$$|R_1^2| = \frac{v_{g2} e^{-\frac{\omega d}{Q v_{g2}}}}{v_{g1}} |R_2^2| = e^{-\frac{\omega d}{Q v_{g1}} - \frac{\omega d}{Q v_{g2}}} |R_2^2|, \tag{A10}$$

$$|R_2^2| = \frac{v_{g3} e^{-\frac{\omega d}{Q v_{g3}}}}{v_{g2}} |R_3^2| = e^{-\frac{\omega d}{Q v_{g2}} - \frac{\omega d}{Q v_{g3}}} |R_3^2|. \tag{A11}$$

The attenuation factors of these three adjacent cells are denoted as $\tau_i = \frac{\omega d}{2Q v_{gi}}$ ($i = 1, 2, 3$). And for a conventional CG structure, τ_i is usually on the order of 10^{-2}, much smaller than one. Therefore, we have the approximations:

$$e^{-\tau_i} \approx 1 - \tau_i, \tag{A12}$$

$$e^{-\tau_1} \approx e^{-\tau_2} \approx e^{-\tau_3} \approx e^{-\tau}, \tag{A13}$$

$$|R_3| + |R_1| \approx |R_2|(2 + \tau_1 - \tau_3) \approx 2|R_2|. \tag{A14}$$

Then Eqs. (4)–(7) are rewritten as follows:

$$\Sigma = \cos\varphi + \frac{j(e^{-2\tau} - e^{2\tau})\sin\varphi}{1 + \frac{1}{|R_2|e^{j\theta}}}, \tag{A15}$$

$$\Delta = -j\sin\varphi \frac{1 - |R_2|e^{j\theta}}{1 + |R_2|e^{j\theta}} + \frac{(e^{-2\tau} - e^{2\tau})\cos\varphi}{1 + \frac{1}{|R_2|e^{j\theta}}}, \tag{A16}$$

$$|R_2| = \left| \frac{\sin\varphi - j\Delta}{\sin\varphi + j(\Delta - (e^{-2\tau} - e^{2\tau})\cos\varphi)} \right|. \tag{A17}$$

The amplitudes of the local reflections for each cell have the relationships as indicated in Eqs. (A10) and (A11). It can be calculated that as the amplitude of local reflection $|R_2|$ for the second cell approaches zero, Δ converges to $-j\sin\varphi$ and the real part of Σ converges to $\cos\varphi$ through Eqs. (A15)–(A17). This is the same as that using Eqs. (4)–(7). Therefore, when $|R|$ is not constant in Eqs. (1)–(3), it does not have any effect on the optimization results.

(ii) When these three consecutive regular cells form a CI structure, the amplitudes of forward fields are attenuated by a factor of $e^{-\tau}$ after traveling through a regular cell. In this case, Eqs. (1)–(3) can be modified as

$$E_1 = E_0(e^{j\varphi} + |R|e^{j(\theta-\varphi)}), \tag{A18}$$

$$E_2 = E_0(e^{-\tau} + e^{\tau}|R|e^{j\theta}), \tag{A19}$$

$$E_3 = E_0(e^{-2\tau}e^{-j\varphi} + e^{2\tau}|R|e^{j(\theta+\varphi)}), \tag{A20}$$

where τ is the attenuation factor for each cell and $R = |R|e^{j\theta}$. Equations (4)–(7) are calculated as

$$\Sigma = \frac{E_3 + E_1}{2E_2} = \frac{\cos(\varphi)(1 + e^{-2\tau}) - j(e^{-2\tau} - 1)\sin\varphi}{2e^{-\tau}} \approx \cos\varphi - j\frac{(e^{-2\tau} - 1)\sin\varphi}{2e^{-\tau}}, \tag{A21}$$

$$\Delta = \frac{E_3 - E_1}{2E_2} = \left(\frac{e^{-2\tau} - 1}{2e^{-\tau}}\cos\varphi + j\frac{e^{-2\tau} + 1}{2e^{-\tau}}\sin\varphi\right) \times \frac{1 - Re^{2\tau}}{1 + Re^{2\tau}} \approx \frac{1 - Re^{2\tau}}{1 + Re^{2\tau}}(-\tau\cos\varphi - j\sin\varphi), \tag{A22}$$

$$Re^{2\tau} = \frac{\sin\varphi - j\tau\cos\varphi - j\Delta}{\sin\varphi - j\tau\cos\varphi + j\Delta}. \tag{A23}$$

Through $R \to 0$ at Eq. (7), we obtain $\Delta \to -j\sin\varphi$, so the local reflection for the second cell is calculated by Eq. (A23):

$$Re^{2\tau} = \frac{-j\tau\cos\varphi}{2\sin\varphi - j\tau\cos\varphi}. \tag{A24}$$

In this situation, there are also local reflections $Re^{-j2\varphi}$ and $Re^{4\tau}e^{j2\varphi}$ generated for the first cell (denoted as 1) and the third cell (denoted as 3), respectively. These reflections result in a poor field flatness inside cells, thereby diluting the accuracy of Kroll method. This means that when $|E_0|$ is not constant for each regular cell, the optimization results are not accurate using Kroll method. To eliminate these reflections, a new criterion is proposed in Sec. II A. This new criterion utilizes the phases of axial electric fields to achieve a high accuracy regardless of the variations of cell geometry and power attenuations. This new criterion can be applied to match any couplers to any TW accelerating structures including CG, CI, and other structures.

APPENDIX B

Based on Ref. [17], the equivalent circuit of a CI structure is depicted in Fig. 12(a). The difference equation and the dispersion can be expressed as

$$I_{p+1} - I_p\left(-\omega^2 LC' + \frac{C'}{C} + 2\right) + I_{p-1} = 0, \tag{B1}$$

$$\omega^2 = \frac{1}{LC} + \frac{2}{LC'}(1 - \cos\varphi). \tag{B2}$$

The characteristic impedance for each regular cell is $Z = \frac{2}{\omega C'}\tan(\frac{\varphi}{2}) \sim (\omega_\pi - \omega_0)$. In a non-CI structure, as shown in Fig. 12(b), the dispersion is modified as follows:

$$\omega_i^2 = \frac{1}{L_i C_i} + \frac{1}{L}\left(\frac{1}{C_i'} + \frac{1}{C_{i+1}'}\right)(1 - \cos\varphi). \tag{B3}$$

In a non-CI structure, the characteristic impedance Z_i for the ith cell ($i = 1, 2, 3, \ldots$) varies linearly and slowly with cells, which results in reflections for each cell. The difference between Z_i and Z_{i+1} is much smaller than Z_i:

$$\frac{Z_i}{Z_{i+1}} \approx \frac{Z_{i+1}}{Z_{i+2}} \approx 1. \tag{B4}$$

A transmission line model is utilized for analyzing a φ-mode structure consisting of n cells, as shown in Fig. 13. The output coupler is matched well, which corresponds to $R_0 = 0$. Here we define:

$$R_f = \frac{\frac{Z_i}{Z_{i+1}} - 1}{\frac{Z_i}{Z_{i+1}} + 1} \approx \frac{\frac{Z_i}{Z_{i+1}} - 1}{2}. \tag{B5}$$

Based on Eq. (B4), R_f can be approximated as a constant value, which is much smaller than one. The reflection at the ith plane R_i can be calculated by the recursive relationship between R_i and R_{i+1}:

$$\begin{aligned} R_{i+1} &= \frac{\frac{Z_i}{Z_{i+1}}\frac{1+R_i e^{2j\varphi}}{1-R_i e^{2j\varphi}} - 1}{\frac{Z_i}{Z_{i+1}}\frac{1+R_i e^{2j\varphi}}{1-R_i e^{2j\varphi}} + 1} \\ &= \frac{(2R_f+1)\left(1 + \frac{2R_i e^{2j\varphi}}{1-R_i e^{2j\varphi}}\right) - 1}{(2R_f+1)\left(1 + \frac{2R_i e^{2j\varphi}}{1-R_i e^{2j\varphi}}\right) + 1}. \end{aligned} \tag{B6}$$

When $R_i \ll 1$ and $R_f \ll 1$, it can be approximated as

$$\begin{aligned} R_{i+1} &\approx \frac{(2R_f+1)(1+2R_i e^{2j\varphi}) - 1}{(2R_f+1)(1+2R_i e^{2j\varphi}) + 1} \\ &= \frac{2R_f + 2R_i e^{2j\varphi} + 4R_i R_f e^{2j\varphi}}{2R_f + 2R_i e^{2j\varphi} + 4R_i R_f e^{2j\varphi} + 2} \\ &\approx R_i e^{2j\varphi} + R_f. \end{aligned} \tag{B7}$$

By further rearranging this recursive relationship, we can obtain:

$$\frac{R_i}{e^{2j\varphi * i}} - \frac{R_{i-1}}{e^{2j\varphi*(i-1)}} = \frac{R_f}{e^{2j\varphi * i}}. \tag{B8}$$

(i) In the case of $R_0 = 0$, R_i can be obtained by summing Eq. (B8) from 1 to i:

$$R_i = \sum_{l=1}^{i} R_f e^{2j(l-1)\varphi} = R_f \frac{1 - e^{2j\varphi * i}}{1 - e^{2j\varphi}}. \tag{B9}$$

It can be derived from Eq. (B9) that when $e^{2j\varphi * i} = 1$, $R_i = 0$. So we get $2\varphi * i = 2p\pi$, where $p = 1, 2, 3, \ldots$. When $\varphi = 120°$ and $i = 3m$ ($m = 1, 2, 3, \ldots$), $R_{3m} \approx 0$. However, in this situation, $R_{3m-1} = -R_f e^{2j\varphi} \neq 0$ and $R_{3m-2} = R_f \neq 0$. The electric fields of the three cells can be expressed by

$$E_{3m-2} = E_{3m-2,0}(1 + R_f), \tag{B10}$$

$$E_{3m-1} = E_{3m-1,0}(1 - R_f e^{2j\varphi}), \tag{B11}$$

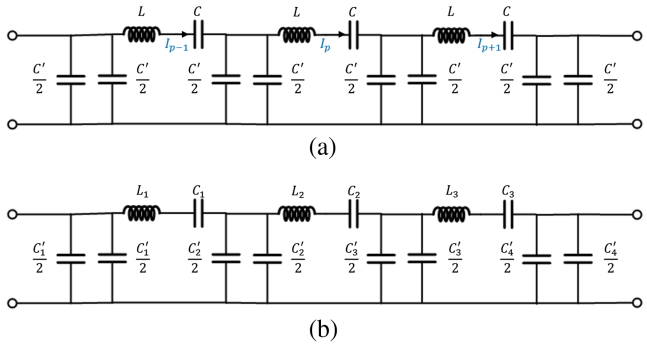

FIG. 12. The equivalent circuits of CI (a) and non-CI (b) structures.

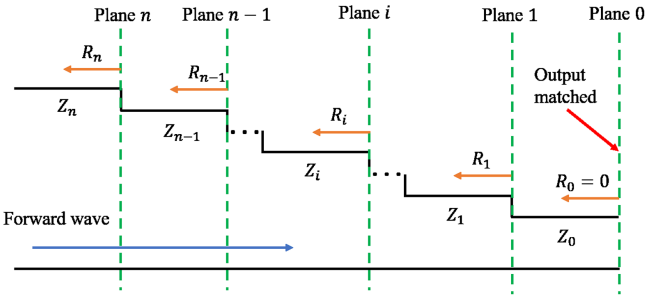

FIG. 13. The transmission line model for a CG structure consisting of n cells with a matched output coupler.

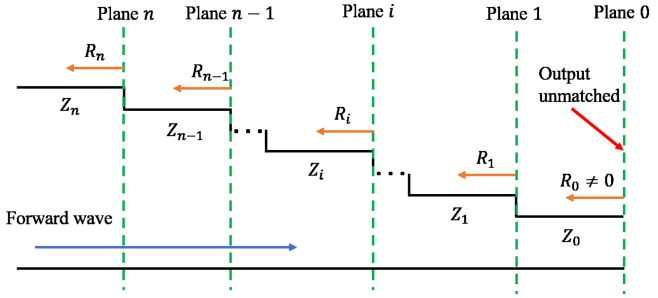

FIG. 14. The transmission line model for a CG structure consisting of n cells with an unmatched output coupler.

$$E_{3m} = E_{3m,0}, \tag{B12}$$

$$E_{3m-2,0} = e^{j\varphi}E_{3m-1,0} = e^{2j\varphi}E_{3m,0}, \tag{B13}$$

where $E_{i,0}$ is the forward electric field of the ith cell. This field distribution means that there are reflections remaining in the adjacent regular cells. These reflections result in a poor field flatness, thereby diluting the accuracy of Kyhl method.

In order to eliminate the reflections, the output coupler has to be unmatched ($R_0 \neq 0$).

(ii) In the case of $R_0 \neq 0$, as shown in Fig. 14, we rearrange Eq. (B7) in a way different from Eq. (B8):

$$R_{i+1} = e^{2j\varphi}R_i + \frac{R_f}{1-e^{2j\varphi}}(1-e^{2j\varphi}), \tag{B14}$$

$$R_{i+1} - \frac{R_f}{1-e^{2j\varphi}} = e^{2j\varphi}\left(R_i - \frac{R_f}{1-e^{2j\varphi}}\right). \tag{B15}$$

It can be found from Eq. (B15) that when $R_0 = \frac{R_f}{1-e^{2j\varphi}}$, R_i is equal to R_0 for any $i \geq 0$ ($i = 0, 1, 2, 3, \ldots, n$). This means that the reflections R_i have the same amplitudes and phases for all of regular cells. So the input coupler has to be carefully designed to cancel the reflections R_n in order to minimize the global reflection coefficient $|S_{11}|$ at the input port. This generates a very good field flatness with correct phase advances between each cell. These analyses can be applied to all non-CI structures including CG and other structures.

[1] P. Emma, R. Akre, J. Arthur *et al.*, First lasing and operation of an ångstrom-wavelength free-electron laser, Nat. Photonics **4**, 641 (2010).

[2] N. Shafqat, C. Serpico, and T. G. Lucas, Design and high-power test of a short prototype of high gradient S-band accelerating structure for the FERMI free electron laser linac upgrade, Nucl. Instrum. Methods Phys. Res. Sect. A **979**, 164473 (2020).

[3] X. Lin, H. Zha, J. Shi *et al.*, Design, fabrication, and testing of low-group-velocity S-band traveling-wave accelerating structure, Nucl. Sci. Tech. **33**, 147 (2022).

[4] H. Ego, T. Abe, Y. Higashi *et al.*, Upgrades of S-band accelerating structures and pulse compressors in the electron and positron injector linac of KEK, in *Proceedings of the 14th International Particle Accelerator Conference, IPAC-2023, Venice, Italy* (JACoW, Geneva, Switzerland, 2023), pp. 2932–2935.

[5] T. Inagaki, C. Kondo, H. Maesaka, T. Ohshima, Y. Otake, T. Sakurai, K. Shirasawa, and T. Shintake, High-gradient C-band linac for a compact X-ray free-electron laser facility, Phys. Rev. ST Accel. Beams **17**, 080702 (2014).

[6] W. Fang, Q. Gu, X. Sheng *et al.*, Design, fabrication and first beam tests of the C-band RF acceleration unit at SINAP, Nucl. Instrum. Methods Phys. Res., Sect. A **823**, 91 (2016).

[7] T. Sakurai, H. Ego, T. Inagaki, T. Asaka, D. Suzuki, S. Miura, and Y. Otake, C-band disk-loaded-type accelerating structure for a high acceleration gradient and high-repetition-rate operation, Phys. Rev. Accel. Beams **20**, 042003 (2017).

[8] D. Alesini, M. Bellaveglia, S. Bini *et al.*, Design of high gradient, high repetition rate damped C-band rf structures, Phys. Rev. Accel. Beams **20**, 032004 (2017).

[9] D. Alesini, M. Bellaveglia, F. Cardelli *et al.*, Realization and high power test of damped C-band accelerating structures, Phys. Rev. Accel. Beams **23**, 042001 (2020).

[10] T. Higo, Progress of X-band accelerating structures, in *Proceedings of the 25th International Linear Accelerator Conference, LINAC-2010, Tsukuba, Japan* (JACoW, Geneva, Switzerland, 2010), pp. 1038–1042.

[11] T. Higo, Y. Higashi, S. Matsumoto *et al.*, Advances in X-band TW accelerator structures operating in the 100 MV/m regime, in *Proceedings of 1st International Particle Accelerator Conference, IPAC-2010, Kyoto, Japan* (JACoW, Geneva, Switzerland, 2010), pp. 3702–3704.

[12] T. Higo, T. Abe, Y. Arakida *et al.*, Comparison of high gradient performance in varying cavity geometries, in *Proceedings of 4th International Particle Accelerator Conference, IPAC-2013, Shanghai, China* (JACoW, Geneva, Switzerland, 2013), pp. 2741–2743.

[13] X. Wu, H. Zha, J. Shi, Huaibi Chen, Tetsuo Abe, Toshiyasu Higo, and Shuji Matsumoto, Design, fabrication, and high-gradient testing of X-band choke-mode damped structures, Phys. Rev. Accel. Beams **22**, 031001 (2019).

[14] C. Nantista, S. Tantawi, and V. Dolgashev, Low-field accelerator structure couplers and design techniques, Phys. Rev. ST Accel. Beams **7**, 072001 (2004).

[15] D. Alesini, Power coupling, arXiv:1112.3201.

[16] E. Westbrook, Microwave impedance matching of feed waveguides to the disk-loaded accelerator structure operating in the $2\pi/3$ mode, Technical Report No. SLAC-TN-63-103, 1963.

[17] M. Chanudet, Matching of the coupler cavity to travelling wave structures at any operating mode, Technical Report No. LAL/RT 93-06, 1993.

[18] D. Alesini, A. Gallo, B. Spataro, A. Marinelli, and L. Palumbo, Design of couplers for traveling wave RF structures using 3D electromagnetic codes in the frequency

domain, Nucl. Instrum. Methods Phys. Res., Sect. A **580**, 1176 (2007).

[19] S. Zheng, Y. Cui, H. Chen, and L. Xiao, A quantitative method of coupler cavity tuning and simulation, in *Proceedings of the 2001 Particle Accelerator Conference, PAC-2001, Chicago, IL* (IEEE, New York, 2001), pp. 981–983.

[20] J. Zhang, Y. Chi, J. Lei *et al.*, Design of a C-band travelling-wave accelerating structure at IHEP, in *Proceedings of the 8th International Particle Accelerator Conference, IPAC-2017, Copenhagen, Denmark* (JACoW, Geneva, Switzerland, 2017), pp. 4196–4199.

[21] C. Ng, K. Ko, and W. Herrmannsfeldt, Modeling accelerator structures and RF Components, AIP Conf. Proc. **297**, 1 (1993).

[22] G. Bowden, W. Fowkes, R. Loewen *et al.*, A compact RF power coupler for the NLC linac, in *Proceedings of the 1999 Particle Accelerator Conference, PAC-1999, New York* (IEEE, New York, 1999), pp. 3426.

[23] N. Kroll, C. Ng, and D. Vier, Applications of time domain simulation to coupler design for periodic structures, in *Proceedings of the 20th International Linear Accelerator Conference, LINAC-2000, Monterey, CA* (SLAC, Menlo Park, CA, 2000), pp. 614–617.

[24] W. Fang, D. Tong, Q. Gu, and Z. Zhao, Design and experimental study of a C-band traveling-wave accelerating structure, Chin. Sci. Bull. **56**, 18 (2011).

[25] A. Grudiev and W. Wuensch, A newly designed and optimized CLIC main linac accelerating structure, in *Proceedings of the 19th International Linear Accelerator Conference, LINAC-2004, Lübeck, Germany* (JACoW, Geneva, Switzerland, 2004), https://accelconf.web.cern.ch/l04/PAPERS/THP72.PDF.

[26] A. Grudiev and W. Wuensch, Design of the CLIC main linac accelerating structure for CLIC Conceptual Design Report, in *Proceedings of the 25th International Linear Accelerator Conference, LINAC-2010, Tsukuba, Japan* (JACoW, Geneva, Switzerland, 2010).

[27] H. Zha and A. Grudiev, Design and optimization of Compact Linear Collider main linac accelerating structure, Phys. Rev. Accel. Beams **19**, 111003 (2016).

[28] H. Zha and A. Grudiev, Design of the Compact Linear Collider main linac accelerating structure made from two halves, Phys. Rev. Accel. Beams **20**, 042001 (2017).

[29] M. Bunge, A general black box theory, Philos. Sci. **30**, 346 (1963).

[30] M. Khan and F. Khan, A comparative study of white box, black box and grey box testing techniques, Int. J. Adv. Comput. Sci. Appl. **3**, 12 (2012).

[31] B. Widrow and M. John, A comparison of adaptive algorithms based on the methods of steepest descent and random search, IEEE Trans. Antennas Propag. **24**, 615 (1976).

[32] P. Baldi, Gradient descent learning algorithm overview: A general dynamical systems perspective, IEEE Trans. Neural Networks **6**, 182 (1995).

[33] J. Moré and D. Thuente, Line search algorithms with guaranteed sufficient decrease, ACM Trans. Math. Softw. **20**, 286 (1994).

[34] M. Rajih, P. Comon, and R. Harshman, Enhanced line search: A novel method to accelerate PARAFAC SIAM, J. Matrix Anal. Appl. **30**, 1128 (2008).

[35] D. Cheng, X. Hu, and T. Shen, *Analysis and Design of Nonlinear Control Systems* (Science Press, Beijing, 2010).

[36] HFSS, www.ansys.com, 2023.